

**Facile one-step solution-phase route to synthesize hollow nanoporous Cu_xO
microcages on 3D copper foam for superior Li storage**

Wenbo Liu,^{a,*} Peng Cheng,^a Xiaomeng Yan,^a Hongmei Gou,^a Shichao Zhang,^b and
Sanqiang Shi^c

^a School of Mechanical Engineering, Sichuan University, Chengdu 610065, China

^b School of Materials Science and Engineering, Beihang University, Beijing 100191,
China

^c Department of Mechanical Engineering, The Hong Kong Polytechnic University,
Hung Hom, Kowloon, Hong Kong

Tel: +86-028-85405320; Fax: +86-028-85403408; E-mail: liuwenbo_8338@163.com.

ABSTRACT

In this report, we develop a simple and effective one-step solution-phase route to in-situ synthesize hollow nanoporous Cu_xO microcages on 3D copper foam. When used as an anode for lithium-ion batteries, the unique 3D electrode exhibits superior Li storage properties with first reversible capacity of 2.82 mAh cm^{-2} and 78.4% capacity retention after 400 cycles at 2 mA cm^{-2} . The excellent electrochemical performance can be ascribed to the stable hollow structure and robust nanoporous shells of Cu_xO microcages, as well as in-situ growth of microcages on copper foam substrate with 3D porous architecture, which is greatly beneficial to buffer large volume change, increase loading mass of active material, boost binding force between active material and substrate, as well as shorten Li^+ and electron migration distance.

KEYWORDS: Solution-phase route; hollow microcages; nanoporous structure; Cu_xO ; Lithium ion battery

■ INTRODUCTION

In recent years, lithium-ion batteries (LIBs) have great advantages of high energy/power density, long cycle life and good safety in use, which can be widely applied in portable electronic devices, pure/hybrid electric vehicles and other modern industrial fields. At present, graphite, as the traditional anode of commercial LIBs, has been increasingly unable to meet the demands of modern society and technology for next-generation LIBs with higher energy density.¹⁻³ Therefore, it needs to be urgent to develop alternative anode materials with high specific capacity. Recently, transition metal oxides have aroused tremendous interest due to their high theoretical capacities from multi-electron reactions with Li^+ and excellent rate performance from the diversity of electrode structure.⁴⁻⁸ Among them, copper(I/II) oxides have the merits of high theoretical capacity, natural abundance, low cost and environmental friendliness, which is expected to be promising anode candidates for advanced LIBs.⁹⁻¹² However, until now, their commercialization still is severely hampered because of poor cycling stability and low coulombic efficiency caused by the large volume variation and low electronic conductivity during cycling.^{13,14}

To address these issues, many strategies have been developed by anode structure design. Especially, introducing the hollow structure is an effective method. Today, researchers have successfully prepared various copper oxides with different hollow structures, such as hollow CuO spheres, hollow Cu₂O cages and hollow CuO/Cu₂O composite polyhedrons by well-developed removable template approaches.¹⁵⁻¹⁷ The stable hollow structure can effectively utilize its internal space to buffer the large

volume change, thus enhancing the cycling stability of the electrode after long cycles.

On the other hand, the development of porous structure can also greatly improve the electrochemical performance of copper oxides.¹⁸⁻²⁰ For example, Yue et al. reported pillow-shaped porous CuO electrode synthesized by controlled thermal decomposition of CuC_2O_4 precursor, which delivered an initial discharge capacity of 2.50 mAh cm^{-1} and 83.3% discharge-capacity retention after 50 cycles at a rate of 0.1 C.²¹ This is mainly attributed to its unique pillow-shaped porous structure, which provides more electrochemical active sites reacting with Li^+ and accelerate organic electrolyte permeation, thus improving the specific capacity.

Enlightened by these, we have reasons to believe that the combination of hollow and porous structures might be a rational way to enhance the Li storage performance. It should be noted that, however, the present hollow or porous electrode materials are usually made into powders and slurries, and then coated on the surfaces of two-dimensional conductive current collectors. It largely leads to the gradual decrease of cycling stability due to the aggregation or pulverization of active materials during repeated charge-discharge processes, which limits their wide application in the near future.²²⁻²³ To overcome above drawbacks, fabricating bulk 3D integrated electrode with hollow porous structure would be a more desirable route to improve its electrochemical and structural durability during a long-cycle process.

Herein, we report a simple and effective one-step solution-phase route to in-situ synthesize hollow nanoporous Cu_xO microcages on 3D copper foam. Compared with conventional template methods or other multi-step synthesis routes, the developed

template-free one-step solution-phase strategy has obvious advantages of simple process, low cost, nearly absolute yield and is suitable for large-scale synthesis. The unique 3D electrode as anode for LIBs exhibits superior Li storage performance with first reversible capacity of 2.82 mAh cm⁻² and 78.4% capacity retention after 400 cycles at a current density of 2 mA cm⁻², which is closely related to the stable hollow structure and robust nanoporous shells of Cu_xO microcages, as well as in-situ growth of microcages on copper foam substrate with 3D porous architecture. We believe that this work can provide a promising anode candidate toward practical application of high-performance LIBs.

■ RESULTS AND DISCUSSION

The hollow nanoporous Cu_xO microcages on 3D copper foam (3D-CF@Cu_xO MCs) can be prepared by a facile one-step solution-phase route by immersing 3D copper foam in a mixed solution of urea and Fe(OH)₃·9H₂O at 90°C, as illustrated in Fig. 1a. The typical reaction times are 6, 12 and 20 h, and the corresponding products are denoted as 3D-CF@Cu_xO MCs-6, 3D-CF@Cu_xO MCs-12 and 3D-CF@Cu_xO MCs-20, respectively. More experimental details can be found in the Supplementary Information. Fig. 1b-d shows the typical SEM and TEM images of 3D-CF@Cu_xO MCs-12. As can be seen clearly in Fig. 1b and its inset, plenty of Cu_xO microcages with uniform sizes can be observed on the surfaces of pore walls of 3D copper foam. In contrast to the bare 3D copper foam substrate (Fig. S1), it is easy to find that these Cu_xO microcages are more prone to grow on flat places rather than backbones (that is intersections of pore walls with different orientations) due to the good binding force

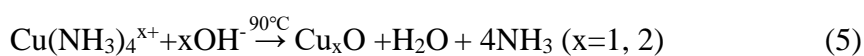
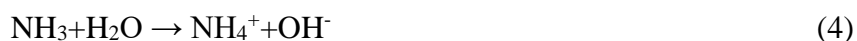
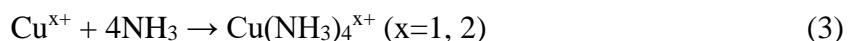
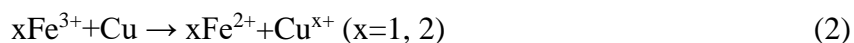
with substrate. Intriguingly, the high-magnification SEM images (Fig. 1c and its inset) of a typical cracked microcage further display that the interior of microcage is hollow structure and its shell is nanoporous structure made of lots of tiny nanoparticles with average sizes of 20-30 nm. All these details can be further confirmed by the TEM observation shown in Fig. 1d. The striking contrast between bright and dark areas indicates that the microcage is typical hollow structure with shell thickness of ca. 150 nm. Meanwhile, the present TEM results also can fully demonstrate that the shell of the hollow microcage is nanoporous structure.

X-ray diffraction (XRD) is conducted to identify the crystal structure of the 3D-CF@Cu_xO MCs-12, as presented in Fig. 1e. The XRD pattern indicates that all the diffraction peaks can be assigned to Cu (PDF No. 04-0836), Cu₂O (PDF No. 05-0667), CuO (PDF No. 44-0706), respectively. No other impurities can be detected, demonstrating the three-phase coexistence in the as-obtained samples. X-ray photoelectron spectroscopy (XPS) is performed to detect the oxidation states of the 3D-CF@Cu_xO MCs-12. From the survey full spectrum, we can find the coexistence of Cu, O and Fe in the as-obtained samples, in which the Fe element may come from the uncleaned Fe³⁺ in solution (Fig. S2). The high-resolution XPS spectrum of Cu 2p in Fig. 1f exhibits that the two peaks at 932.35 and 952.24 eV correspond to the Cu 2p_{3/2} and Cu 2p_{1/2} peaks of Cu(I) in Cu₂O, while the other two peaks at 934.24 and 954.22 eV designate to the Cu 2p_{3/2} and Cu 2p_{1/2} peaks of Cu(II) in CuO.²⁴ The high-resolution XPS spectrum of O 1s in Fig. 1g can be fitted into four peaks. The two peaks at 529.26 and 529.99 eV correspond to lattice oxygen within CuO and

Cu₂O, while the other two peaks at 531.02 and 532.71 eV may originate from O₂ and H₂O adsorbed physically on sample surfaces.^{25,26} Evidently, the present XPS results further confirm the coexistence of Cu₂O and CuO in the samples, in good agreement with the XRD analysis above.

To further understand the formation mechanism, the microstructure evolution of 3D-CF@Cu_xO MCs was investigated systematically by characterizing the products obtained after different reaction times. Fig. 2 shows the representative SEM images of 3D-CF@Cu_xO MCs obtained at 90°C for 6, 12 and 20 h, respectively. The reaction time was found to be crucial to achieve the ideal hollow nanoporous structure of microcage. It can be seen that when the reaction time is 6 h, just a number of solid microcubes can be prepared on the surfaces of 3D copper foam substrates (Fig. 2a). With the reaction time extending to 12 h, it is interesting that these solid microcubes can be gradually transformed into hollow microcages with uniform nanoporous shells (Fig. 2b). As the reaction time further increases (20 h), the nanoporous shells of these hollow microcages continually coarsen and eventually severely collapse (Fig. 2c). Note that, in Fig. 2b-c, the hollow structure of Cu_xO MCs can be intuitively judged by the partial collapse at the center of nanoporous shells, whereas those small-sized (<1 μm) Cu_xO MCs often without the partial collapse phenomenon still have the hollow structure in nature, which can be well confirmed by TEM observation in Fig. 1d. The phase composition of products with different reaction times is further examined by XRD, which indicates the coexistence of Cu, Cu₂O and CuO in all these samples (Fig. S3). As a result, it can be reasonable to believe that in the formation process of

3D-CF@Cu_xO MCs, the phase composition remains unchanged but only the structure evolves. We speculate that the evolution law involves three main processes. (1) During the initial reaction stage (0~6 h), copper oxide nanoparticles quickly aggregate to reduce the overall energy of system and self-assemble into solid microcubes.²⁷ (2) During the subsequent reaction stage (6~12 h), the solid microcubes gradually hollow inside and then evolve into hollow nanoporous microcages through Ostwald ripening effect.²⁸ (3) During the over-reaction stage (12~20 h), the nanoporous shells of hollow microcages constantly coarsen and finally severely collapse at the center of nanoporous shells due to rapid diffusion of surface atoms of nanoporous shells in solution driven by elevated temperature. Additionally, the probable formation mechanism of copper oxides is as follows. The urea was hydrolyzed into NH₃·H₂O at 90°C and meanwhile, copper atoms on the surfaces of copper foams can be oxidated to Cu^{x+} (x=1, 2) by reduction of Fe³⁺ in the Fe(NO₃)₃·9H₂O solution.²⁹ Then, the copper oxides can be obtained by the transformation of Cu(NH₃)₄^{x+} complex ions, which are formed by the combination of NH₃ and Cu^{x+} (x=1, 2).³⁰ The main reactions involved are shown below:



Besides, to explore the key forming factors in the one-step solution-phase route, the

same experimental procedure was also carried out on various substrates with different components and structures, such as 3D nickel foam, 2D copper foil, 2D 304 stainless steel sheet, and 2D SiC ceramic chip. The typical SEM images were illustrated in Fig. S4. Clearly, just can on 2D copper foil substrate observe hollow nanoporous microcages similar to those on 3D copper foams, indicating the key forming factor just is component Cu and has nothing to do with substrate structures, such as shape, curvature, roughness and so on. Evidently, compared to the 2D Cu foil substrates used in commercial cells, the chosen 3D Cu foams with larger specific surface areas can grow more microcages as active material to effectively boost Li storage capability of electrodes.³¹⁻³⁴ In addition, it has been found that the synergistic effect of urea and $\text{Fe}(\text{NO}_3)_3 \cdot 9\text{H}_2\text{O}$ in the solution is also greatly important for the formation of hollow nanoporous microcages. The 3D copper foam was attempted to immerse in a single urea or $\text{Fe}(\text{NO}_3)_3 \cdot 9\text{H}_2\text{O}$ solution under the same experimental conditions, but the microcages cannot be obtained (Fig. S5).

The electrochemical performance of 3D-CF@Cu_xO MCs-12 electrode is presented in Fig. 3. Fig. 3a shows the continuous CVs measured at a scan rate of 0.1 mV s⁻¹ in the potential range of 0.01-3.0 V (vs. Li/Li⁺), in which the open circuit voltage (OCV) is ca. 2.12 V (vs. Li/Li⁺). During the first discharge process, three reduction peaks are observed clearly at 1.58, 1.05 and 0.67 V (vs. Li/Li⁺). The peak at 1.58 V (vs. Li/Li⁺) can be attributed to the transformation of CuO to an intermediate composite copper oxide solid solution ($\text{Cu}^{\text{II}}_{1-x}\text{Cu}^{\text{I}}\text{O}_{1-x/2}$ ($0 < x < 0.4$)).³⁵ The peak at 1.05 V (vs. Li/Li⁺) corresponds to the further conversion from the copper oxide solid solution to

Cu₂O.^{35,36} The big and broad peak at 0.67 V (vs. Li/Li⁺) is ascribed to the transformation from Cu₂O to Cu along with the growth of solid electrolyte interface (SEI) films.³⁷ In contrast, during the first charge process, three oxidation peaks can be observed at 1.15, 1.66 and 2.52 V (vs. Li/Li⁺), assigning to the partial decomposition of SEI films, as well as the multistep reversible transformation of Cu to Cu₂O and CuO, respectively.^{38,39} It is worth noting that the oxidation peak of SEI films located at 1.15 V (vs. Li/Li⁺) is very small and almost disappears after the 1st cycle, suggesting its good stability. Moreover, the subsequent CV curves are just completely overlapped with each other, indicating the excellent electrochemical reversibility of the electrode.

Fig. 3b illustrates the cycle performance of 3D-CF@Cu_xO MCs-12 electrode at 2 mA cm⁻²; meanwhile, the counterparts of 3D-CF@Cu_xO MCs-6 and 3D-CF@Cu_xO MCs-20 electrodes are also added for clear comparison. For 3D-CF@Cu_xO MCs-12 electrode, the charge and discharge specific capacities slightly decrease in the initial 20 cycles and then tend to be stable, finally remaining the reversible capacity of 2.21 mAh cm⁻² after 400 cycles with 78.4% capacity retention. Note that the initial coulombic efficiency is just ca. 43%, which mainly stems from the partial irreversible conversion of copper oxides, formation of SEI films and interfacial spaces consuming lots of Li⁺.³⁸ In fact, this phenomenon can be found in most TMOs-based electrode materials.^{40,41} Except for the first several cycles, the coulombic efficiency is always >99.7 %, indicative of its good electrochemical reversibility. In contrast, the 3D-CF@Cu_xO MCs-6 and 3D-CF@Cu_xO MCs-20 electrodes just deliver the

reversible capacities of 1.48 mAh cm^{-2} after 200 cycles with 73.3% capacity retention and 1.17 mAh cm^{-2} after 150 cycles with 53.4% capacity retention, respectively. Obviously, compared to the 3D-CF@Cu_xO MCs-6 and 3D-CF@Cu_xO MCs-20 electrodes, the 3D-CF@Cu_xO MCs-12 electrode exhibits higher reversible capacity, longer cycle life and better cycling stability, implying that the ideal hollow nanoporous structure of microcage plays a key role in improving the Li storage performance. Firstly, the stable hollow structure inside microcages can offer ample rooms to alleviate the large volume and structure changes during cycling. Secondly, the robust nanoporous shells of microcages can promote fast permeation of organic electrolyte and provide sufficient active sites for Li⁺ insertion and extraction. It is worth noting that the arrangement of Cu_xO MCs on 3D copper foam may not be a main factor to affect its electrochemical behavior because the similar electrochemical properties always can be obtained steadily for the 3D-CF@Cu_xO MCs-12 electrodes with different random arrangements of Cu_xO MCs, indicating its good reproducibility. Additionally, a comparison of Li storage properties of various Cu_xO-based electrode materials with different structure designs reported in the recent literature has been listed in detail in Table S1. Obviously, the higher areal capacity and longer cycle life can be achieved well in the 3D-CF@Cu_xO MCs electrode.

The rate capability of the 3D-CF@Cu_xO MCs-12 electrode was further investigated under different current densities, as displayed in Fig. 3c. Clearly, the large reversible specific capacities of 3.07, 2.03, 1.51 and 1.07 mAh cm^{-2} can be achieved after every 10 cycles at current densities of 1, 2, 4 and 8 mA cm^{-2} , respectively. When the current

density returns to the initial value (1 mA cm^{-2}), the reversible capacity can quickly increase to 2.78 mAh cm^{-2} , maintaining as high as ca. 90.6% capacity retention. Even after undergoing various high-rate cycles, the 3D-CF@Cu_xO MCs-12 electrode still can deliver a relatively large reversible capacity of 2.45 mAh cm^{-2} after 120 cycles, indicating its superior rate capability. This can be ascribed to the structure design in nanoporous shells of hollow microcages, which greatly facilitates to provide more Li⁺/electron transfer channels and shorten Li⁺ diffusion distance in active material. This can be further discussed on a basis of the EIS results in the following part.

The Nyquist plots of the 3D-CF@Cu_xO MCs-12 electrode before and after 400 cycles were tested, as presented in Fig. 3d, in which the compressed semicircle in high-medium frequency region stands for charge transfer resistance (R_{ct}) related to the electrochemical reactions on electrode/electrolyte interfaces. Obviously, compared to the counterpart (ca. $150 \ \Omega$) before cycling, the R_{ct} value of the 3D-CF@Cu_xO MCs-12 electrode after 400 cycles can be identified to be just ca. $105 \ \Omega$, suggesting the better Li⁺ and electron transport abilities in the 3D-CF@Cu_xO MCs-12 electrode. The present EIS results clearly demonstrate that the unique 3D electrode structure (including a 3D porous substrate, even distribution of hollow microcages and good binding force between them by in-situ growth) is significantly beneficial for rapid Li⁺ diffusion, electron transport and electrode/electrolyte wettability.

Fig. 4a-b shows the SEM images of the 3D-CF@Cu_xO MCs-12 electrode after 400 cycles. Clearly, the microstructure of the 3D-CF@Cu_xO MCs-12 electrode after cycling has little change relative to that before cycling (Fig. 4a). Especially, the

microcages are still evenly distributed on 3D copper foam substrate without the visible aggregation, pulverization or exfoliation (inset in part a). Moreover, the high-magnification SEM image in Fig. 4b further exhibits that the shells of hollow microcages still maintain good nanoporous structure and no obvious damage or collapse take place after 400 cycles, indicating its good mechanical integrity and structure stability. The superior electrochemical performance of 3D-CF@Cu_xO MCs-12 electrode by the one-step solution-phase route demonstrates the essential merits of in-situ growth of hollow nanoporous Cu_xO microcages on 3D copper foam substrate, as illustrated in Fig. 4c. (I) The stable microcages with ample hollow structure can effectively buffer the large volume and structure changes during repeated lithiation-delithiation processes, improving the cycling ability. (II) The nanoporous shells of microcages can offer more Li⁺ and electron transfer channels as well as shorten Li⁺ diffusion distance in active material, boosting the rate capability. (III) The copper foam as 3D substrate with micron-sized porous structure can grow more active materials and increase contact areas between electrolyte and electrode, enhancing the areal capacity of the electrode. (IV) The in-situ growth of microcages on copper foam without use of binders and conductive agents can markedly increase the binding force and further ameliorate energy and power densities.

■ CONCLUSION

A simple and effective one-step solution-phase route has been developed to in-situ prepare hollow nanoporous Cu_xO microcages on 3D copper foam substrate. As an anode for LIBs, the unique 3D electrode exhibits excellent Li storage properties with

first reversible capacity of 2.82 mAh cm⁻², 78.4% capacity retention and > 99.7% coulombic efficiency after 400 cycles. The good electrochemical performance can be closely related to the the stable hollow structure and robust nanoporous shells of Cu_xO microcages, as well as in-situ growth of microcages on 3D copper foam substrate with micron-sized porous architecture.

■ ASSOCIATED CONTENT

Supporting Information

The Supporting Information is available free of charge on the ACS Publications website at <http://pubs.acs.org>.

Experimental material and method; SEM images of bare 3D copper foam substrate; XPS survey spectrum of the 3D-CF@Cu_xO MCs-12 electrode; XRD patterns of the 3D-CF@Cu_xO MCs-6, 3D-CF@Cu_xO MCs-12 and 3D-CF@Cu_xO MCs-20 electrodes; Surface micromorphology of 3D nickel foam, 2D copper foil, 2D 304 stainless steel sheet, and 2D SiC ceramic chip as substrates; SEM images of surfaces of 3D copper foam immersing in a single urea and Fe(NO₃)₃·9H₂O solution under the same experimental conditions; A detailed comparison of Li storage performance of various Cu_xO-based nanocomposites with different structure designs as anodes for LIBs.

■ AUTHOR INFORMATION

Corresponding Author

*E-mail: liuwenbo_8338@163.com.

Author Contributions

W.L. directed the project and designed the experiments. P.C., X.Y. and H.G. carried

out the experiments and analyzed the data. W.L. wrote the main manuscript text, S.S. and S.Z. added some useful advice. All authors discussed the results and reviewed the manuscript.

Notes

The authors declare no competing financial interest.

■ ACKNOWLEDGMENTS

We give thanks to financial support by the National Natural Science Foundation of China (52075351, 51604177), the National Key Research and Development Program of China (2019YFA0705701), the International S&T Innovation Cooperation Program of Sichuan Province (2020YFH0039), the Chengdu International S&T Cooperation Funded Project (2019-GH02-00015-HZ, 2020-GH02-00006-HZ), the “1000 Talents Plan” of Sichuan Province, the Experimental Technology Project of Sichuan University (20200080), and the Talent Introduction Program of Sichuan University (YJ201410). Additionally, the authors specially thank Dr. Shanling Wang (Analytical & Testing Center, Sichuan University) for help in TEM characterization.

■ REFERENCES

- (1) Zheng, S. S. The effect of the charging protocol on the cycle life of a Li-ion battery. *J. Power Sources* **2006**, *161*, 1385-1391.
- (2) Liu, W. B.; Chen, X.; Zhang, J. Z.; Zhang, S. C.; Shi, S. Q. In-situ synthesis of freestanding porous SnO_x-decorated Ni₃Sn₂ composites with enhanced Li storage properties. *Chem. Eng. J.* **2021**, *412*, 128591.
- (3) Dong, X.; Liu, W. B.; Chen, X.; Yan, J. Z.; Li, N.; Shi, S. Q.; Zhang, S. C.; Yang,

- X. S. Novel three dimensional hierarchical porous Sn-Ni alloys as anode for lithium ion batteries with long cycle life by pulse electrodeposition. *Chem. Eng. J.* **2018**, *350*, 791-798.
- (4) Poizot, P.; Laruelle, S.; Grugeon, S.; Dupont, L.; Tarascon, J. M. Nano-sized transition-metal oxides as negative-electrode materials for lithium-ion batteries. *Nature* **2000**, *407*, 496-499.
- (5) Nitta, N.; Wu, F. X.; Lee, J. T.; Yushin, G. Li ion battery materials: present and future. *Mater. Today* **2015**, *18*, 252-264.
- (6) Park, J. C.; Kim, J.; Kwon, H.; Song, H. Gram-Scale Synthesis of Cu₂O nanocubes and subsequent oxidation to CuO hollow nanostructures for lithium-ion battery anode materials. *Adv. Mater.* **2009**, *21*, 803-807.
- (7) Dong, Y.; Md, K.; Chui, Y. S.; Xia, Y.; Cao, C.; Lee, J. M.; Zapien, J. A. Synthesis of CNT@Fe₃O₄-C hybrid nanocables as anode materials with enhanced electrochemical performance for lithium ion batteries. *Electrochim. Acta* **2015**, *176*, 1332-1337.
- (8) Zhang, N.; Han, X.; Liu, Y.; Hu, X.; Zhao, Q.; Chen, J. 3D porous-Fe₂O₃@C nanocomposite as high-performance anode material of na-ion batteries. *Adv. Energy Mater.* **2015**, *5*, 1-7.
- (9) Chen, W. Q.; Zhang, W. F.; Chen, L.; Zeng, L. X.; Wei, M. D. Facile synthesis of Cu₂O nanorod arrays on Cu foam as a self-supporting anode material for lithium ion batteries. *J. Alloys Compd.* **2017**, *723*, 172-178.
- (10) Han, F.; Li, D.; Li, W. C.; Lei, C.; Sun, Q.; Lu, A. H. Nanoengineered

polypyrrole-coated Fe₂O₃@C multifunctional composites with an improved cycle stability as lithium-ion anodes. *Adv. Funct. Mater.* **2013**, *23*, 1692-1700.

(11) Lou, P.; Cui, Z.; Jia, Z.; Sun, J.; Tan, Y.; Guo, X. Monodispersed carbon-coated cubic NiP₂ nanoparticles anchored on carbon nanotubes as ultra-long-life anodes for reversible lithium storage, *ACS Nano* **2017**, *11*, 3705-3715.

(12) Wang, C.; Wu, L. X.; Wang, H.; Zuo, W. H.; Li, Y. Y.; Liu, J. P. Fabrication and shell optimization of synergistic TiO₂-MoO₃ core-shell nanowire array anode for high energy and power density lithium-ion batteries. *Adv. Funct. Mater.* **2015**, *25*, 3524-3533.

(13) Sun, L. N.; Deng, Q. W.; Li, Y. L.; Deng, L. B.; Wang, Y. Y.; Ren, X. Z.; Zhang, P. X. Solvothermal synthesis of ternary Cu₂O-CuO-RGO composites as anode materials for high performance lithium-ion batteries. *Electrochim. Acta* **2016**, *222*, 1650-1659.

(14) Zhang, S.; Liu, H.; Sun, C.; Liu, P.; Li, L.; Yang, Z.; Feng, X.; Huo, F.; Lu, X.; CuO/Cu₂O porous composites: shape and composition controllable fabrication inherited from metal organic frameworks and further application in CO oxidation. *J. Mater. Chem. A* **2015**, *3*, 5294-5298.

(15) Kong, M.; Zhang, W. X.; Yang, Z. H.; Weng, S. Y.; Chen, Z. X. Facile synthesis of CuO hollow nanospheres assembled by nanoparticles and their electrochemical performance. *Appl. Surf. Sci.* **2011**, *258*, 1317-1321.

(16) Lyu, F.; Li, M.; Wang, Z.; Nan, B.; Wu, S.; Cao, L.; Sun, Z.; Yang, M.; Wang, W.; Shang, C.; Lu, Z. Supramolecular hydrogel directed self-assembly of C-and N-doped

hollow CuO as high-performance anode materials for Li-ion batteries. *Chem. Commun.* **2017**, 53, 2138-2141.

(17) Hu, L.; Huang, Y. M.; Zhang, F. P.; Chen, Q. W. CuO/Cu₂O composite hollow polyhedrons fabricated from metal-organic framework templates for lithium-ion battery anodes with a long cycling life. *Nanoscale* **2013**, 5, 4186-4190.

(18) Zhang, Z. L.; Chen, H.; She, X. L.; Sun, J.; Teo, J.; Su, F. B. Synthesis of mesoporous copper oxide microspheres with different surface areas and their lithium storage properties. *J. Power Sources* **2012**, 217, 336-344.

(19) Liu, W. B.; Chen, L.; Cui, L.; Yan, J. Z.; Zhang, S. C.; Shi, S. Q. Freestanding 3D nanoporous Cu@1D Cu₂O nanowire heterostructure: From facile one-step protocol to robust application in Li storage. *J. Mater. Chem. A* **2019**, 7, 15089-15100.

(20) Ko, S.; Lee, J.-I.; Yang, H.S.; Park, S.; Jeong, U. Mesoporous CuO particles threaded with CNTs for high-performance lithium-ion battery anodes. *Adv. Mater.* **2012**, 24, 4451-4456.

(21) Wan, M.; Jin, D. L.; Feng, R.; Si, L. M.; Gao, M. X.; Yue, L. H. Pillow-shaped porous CuO as anode material for lithium-ion batteries. *Inorg. Chem. Commun.* **2011**, 14, 38-41.

(22) Y. Sun, S. Jiang, W. Bi, C. Wu, Y. Xie, Highly ordered lamellar V₂O₃-based hybrid nanorods towards superior aqueous lithium-ion battery performance. *J. Power Sources* **2011**, 196, 8644-8650.

(23) Yang, Y.; Liu, S.; Bian, X.; Feng, J.; An, Y.; Yuan, C. Morphology- and porosity-tunable synthesis of 3D-nanoporous SiGe alloy as high-performance

lithium-ion battery anode. *ACS Nano* **2018**, *12*, 2900-2908.

(24) Chen, W. Q.; Zhang, W. F.; Chen, L.; Zeng, L. X.; Wei, M. D. Facile synthesis of Cu₂O nanorod arrays on Cu foam as a self-supporting anode material for lithium ion batteries. *J. Alloys Compd.* **2017**, *723*, 172-178.

(25) Liu, S.; Hou, H. Y.; Liu, X. X.; Duan, J. X.; Yao, Y.; Liao, Q. S. High-performance hierarchical cypress-like CuO/Cu₂O/Cu anode for lithium ion battery. *Ionics* **2017**, *23*, 1075-1082.

(26) Devaraj, M.; Deivasigmani, R. K.; Jeyadevan, S. Enhancement of the electrochemical behavior of CuO nanoleaves on MWCNTs/GC composite film modified electrode for determination of norfloxacin. *Colloids Surf. B* **2013**, *102*, 554-561.

(27) Wang, Z. H.; Wang, H.; Wang, L. L.; Pan, L. One-pot synthesis of single-crystalline Cu₂O hollow nanocubes. *J. Phys. Chem. Solids.* **2009**, *70*, 719-722.

(28) Ostwald, W. Z. Studies on the formation and transformation of solid phases. *Phys. Chem.* **1897**, *22*, 289-330.

(29) Wang, Z. Y.; Luan, D. Y.; Madhavi, S.; Li, C. M.; Lou, X. W. α -Fe₂O₃ nanotubes with superior lithium storage capability. *Chem. Commun.* **2011**, *47*, 8061-8063.

(30) Li, Y.; Tan, B.; Wu, Y. Ammonia-evaporation-induced synthetic method for metal (Cu, Zn, Cd, Ni) hydroxide/oxide nanostructures. *Chem. Mater.* **2008**, *20*, 567-576.

(31) Zhang, X.; Liu, T.; Zhang, S. F.; Huang, X.; Xu, B.Q.; Lin, Y. H.; Xu, B.; Li, L. L.; Nan, C. W.; Shen, Y. Synergistic Coupling between Li_{6.75}La₃Zr_{1.75}Ta_{0.25}O₁₂ and

Poly(vinylidene fluoride) Induces High Ionic Conductivity, Mechanical Strength, and Thermal Stability of Solid Composite Electrolytes. *J. Am. Chem. Soc.* **2017**, *139*, 13779-13785.

(32) Zegeye, T. A.; Su, W. N.; Fenta, F. W.; Zeleke, T. S.; Jiang, S. K.; Hwang, B. J. Ultrathin $\text{Li}_{6.75}\text{La}_3\text{Zr}_{1.75}\text{Ta}_{0.25}\text{O}_{12}$ -Based Composite Solid Electrolytes Laminated on Anode and Cathode Surfaces for Anode-free Lithium Metal Batteries. *ACS Appl. Energy Mater.* **2020**, *3*(12), 11713-11723.

(33) Liu, W. B.; Zhang, S. C.; Li, N.; Zheng, J. W.; An, S. S.; Xing, Y. L. Monolithic nanoporous copper ribbons from Mg-Cu alloys with copper contents below 33 at.%: Fabrication, structure evolution and coarsening behavior along the thickness direction. *Int. J. Electrochem. Sci.* **2011**, *6*, 5445-5461.

(34) Liu, W. B.; Zhang, S. C.; Li, N.; Zheng, J. W.; An, S. S.; Li, G. X. Influence of dealloying solution on the microstructure of monolithic nanoporous copper through chemical dealloying of Al 30 at.% Cu alloy. *Int. J. Electrochem. Sci.* **2012**, *7*, 7993-8006.

(35) Zhang, J.; Zhang, M.; Zhang, L. Binder-free three-dimensional porous structured metal oxides as anode for high performance lithium-ion battery. *Electrochim. Acta* **2013**, *105*, 282-288.

(36) Zhou, X. Y.; Zhang, J.; Su, Q. M.; Shi, J. J.; Liu, Y.; Du, G. H. Nanoleaf-on-sheet CuO/graphene composites: Microwave-assisted assemble and excellent electrochemical performances for lithium ion batteries. *Electrochim. Acta* **2014**, *125*, 615-621.

- (37) Hu, X.; Li, C.; Lou, X.; Yang, Q.; Hu, B. Hierarchical CuO octahedra inherited from copper metal-organic frameworks: high-rate and high-capacity lithium-ion storage materials stimulated by pseudocapacitance. *J. Mater. Chem. A* **2017**, *5*, 12828-12837.
- (38) Xiang, J. Y.; Tu, J. P.; Yuan, Y. F.; Huang, X. H.; Zhou, Y.; Zhang, L. Improved electrochemical performances of core-shell Cu₂O/Cu composite prepared by a simple one-step method. *Electrochem. Commun.* **2009**, *11*, 262-265.
- (39) Yuan, W.; Qiu, Z.; Chen, Y.; Zhao, B.; Liu, M.; Tang, Y. A binder-free composite anode composed of CuO nanosheets and multi-wall carbon nanotubes for high-performance lithium-ion batteries. *Electrochim. Acta* **2018**, *267*, 150-160.
- (40) Liang, P.; Zhang, H.; Su, Y.; Huang, Z.; Wang, C. A.; Zhong, M. In situ preparation of a binder-free nano-cotton-like CuO-Cu integrated anode on a current collector by laser ablation oxidation for long cycle life Li-ion batteries. *J. Mater. Chem. A* **2017**, *5*, 19781-19789.
- (41) Reddy, M. V.; Yu, T.; Sow, C. H.; Shen, Z. X.; Lim, C. T.; Rao, G. V.; Chowdari, B. V. R. α -Fe₂O₃ nanoflakes as an anode material for Li-ion batteries. *Adv. Funct. Mater.* **2007**, *17*, 2792-2799.

Figure Captions:

Fig. 1. Fabrication and structure characterization of 3D-CF@Cu_xO MCs electrode. (a) Schematic of preparation process of the 3D-CF@Cu_xO MCs electrode. (b-c) Typical SEM images of the 3D-CF@Cu_xO MCs-12 electrode, in which the insets in part b and c are the low-magnification image of the electrode and locally magnified image of nanoporous shells of the Cu_xO microcages. (d) Typical TEM image of hollow nanoporous Cu_xO microcages. (e) XRD pattern of the 3D-CF@Cu_xO MCs-12 electrode. (f-g) High-resolution XPS spectra of Cu 2p and O 1s for the 3D-CF@Cu_xO MCs-12 electrode.

Fig. 2. Structure evolution and formation mechanism of 3D-CF@Cu_xO MCs electrode. SEM images of (a) the 3D-CF@Cu_xO MCs-6, (b) the 3D-CF@Cu_xO MCs-12 and (c) the 3D-CF@Cu_xO MCs-20 electrodes, respectively.

Fig. 3. Electrochemical performance of 3D-CF@Cu_xO MCs electrode as anode for LIBs. (a) CVs of the 3D-CF@Cu_xO MCs-12 electrode for the first three cycles ranging from 0.01 to 3.0 V (vs. Li/Li⁺) at a scan rate of 0.1 mV s⁻¹. (b) Cycle performance of the 3D-CF@Cu_xO MCs-6, 3D-CF@Cu_xO MCs-12 and 3D-CF@Cu_xO MCs-20 electrodes at a current density of 2 mA cm⁻². (c) Rate capability profiles of the 3D-CF@Cu_xO MCs-12 electrode at current densities of 1, 2, 4, and 8 mA cm⁻². (d) Nyquist plots of the 3D-CF@Cu_xO MCs-12 electrode before cycling and after 400 cycles.

Fig. 4. Structure characterization after cycling and lithium storage mechanism of 3D-CF@Cu_xO MCs electrode. (a-b) SEM images of the 3D-CF@Cu_xO MCs-12

electrode after 400 charge-discharge cycles, in which the inset in part a is the corresponding low-magnification SEM image. (c) Schematic illustration for lithiation-delithiation reaction of the 3D-CF@Cu_xO MCs-12 electrode.

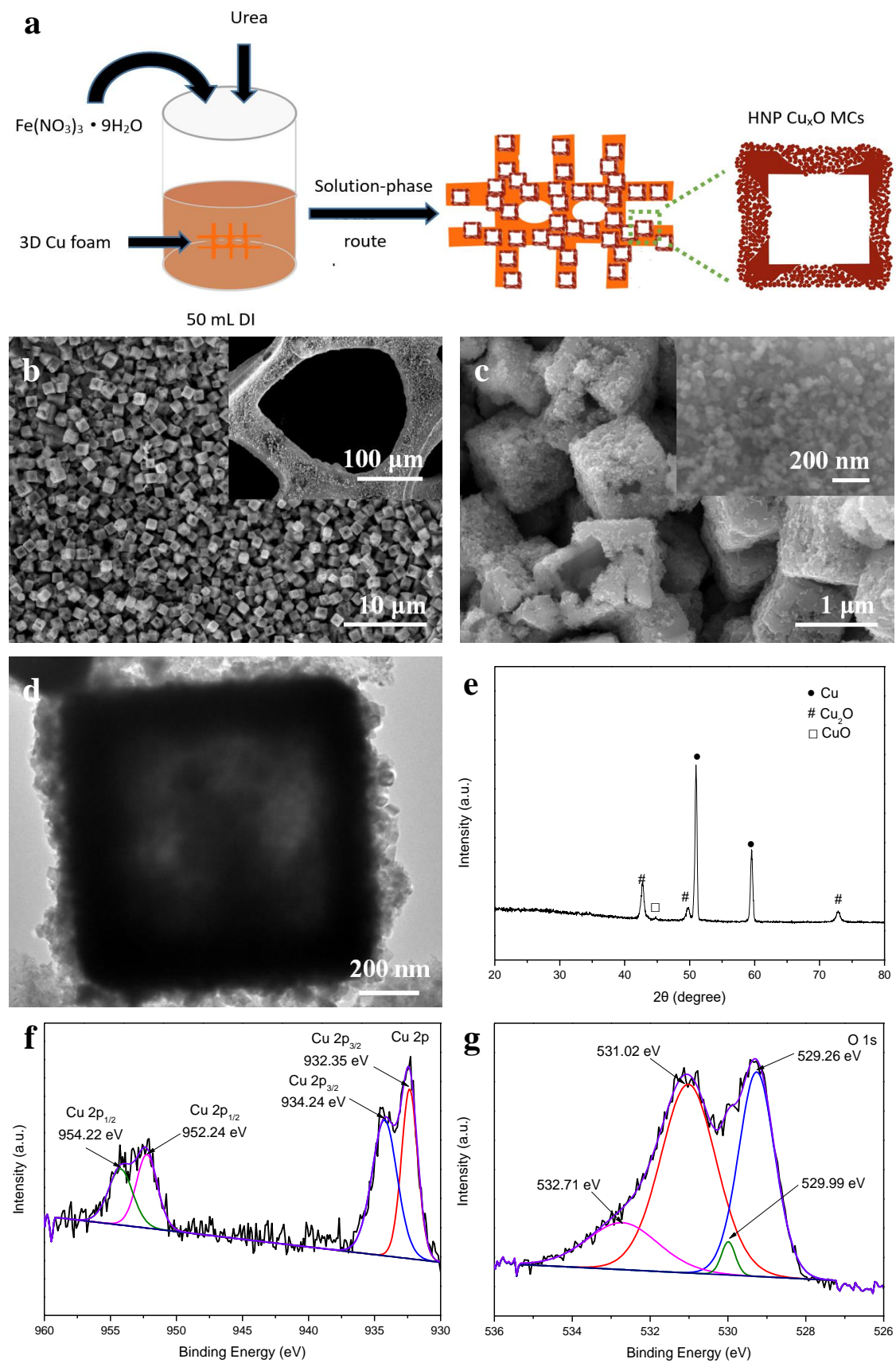


Fig. 1. Fabrication and structure characterization of 3D-CF@ Cu_xO MCs electrode. (a) Schematic of preparation process of the 3D-CF@ Cu_xO MCs electrode.

(b-c) Typical SEM images of the 3D-CF@Cu_xO MCs-12 electrode, in which the insets in part b and c are the low-magnification image of the electrode and locally magnified image of nanoporous shells of the Cu_xO microcages. (d) Typical TEM image of hollow nanoporous Cu_xO microcages. (e) XRD pattern of the 3D-CF@Cu_xO MCs-12 electrode. (f-g) High-resolution XPS spectra of Cu 2p and O 1s for the 3D-CF@Cu_xO MCs-12 electrode.

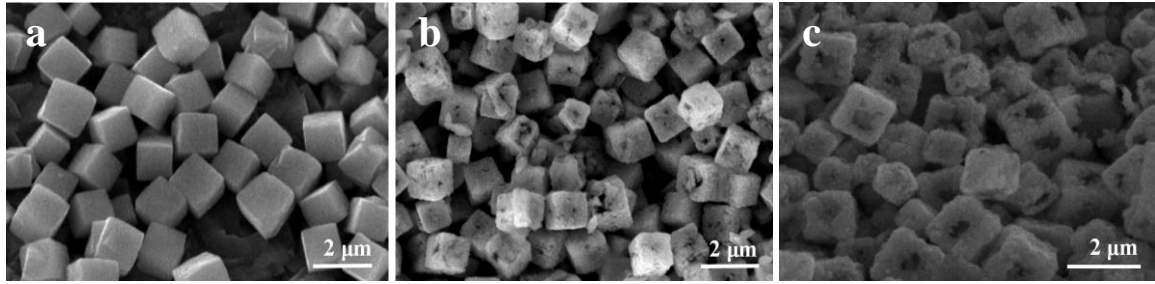


Fig. 2. Structure evolution and formation mechanism of 3D-CF@Cu_xO MCs electrode. SEM images of (a) the 3D-CF@Cu_xO MCs-6, (b) the 3D-CF@Cu_xO MCs-12 and (c) the 3D-CF@Cu_xO MCs-20 electrodes, respectively.

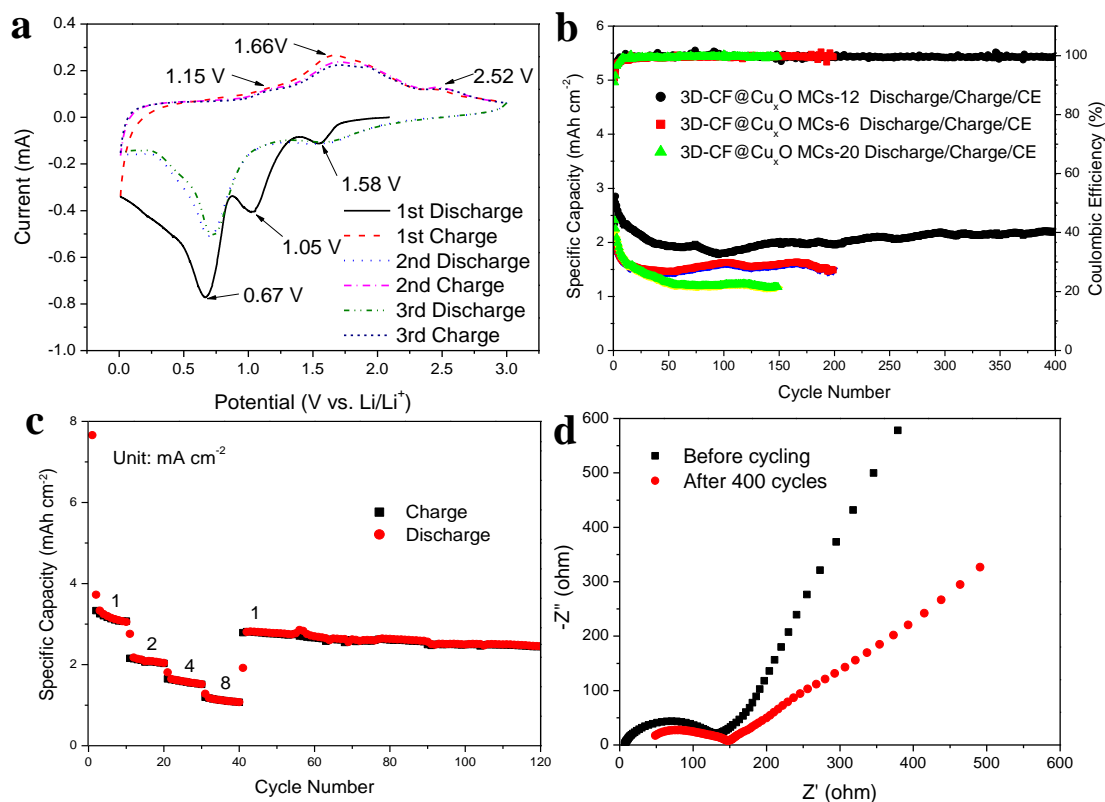


Fig. 3. Electrochemical performance of 3D-CF@Cu_xO MCs electrode as anode for LIBs. (a) CVs of the 3D-CF@Cu_xO MCs-12 electrode for the first three cycles ranging from 0.01 to 3.0 V (vs. Li/Li⁺) at a scan rate of 0.1 mV s⁻¹. (b) Cycle performance of the 3D-CF@Cu_xO MCs-6, 3D-CF@Cu_xO MCs-12 and 3D-CF@Cu_xO MCs-20 electrodes at a current density of 2 mA cm⁻². (c) Rate capability profiles of the 3D-CF@Cu_xO MCs-12 electrode at current densities of 1, 2, 4, and 8 mA cm⁻². (d) Nyquist plots of the 3D-CF@Cu_xO MCs-12 electrode before cycling and after 400 cycles.

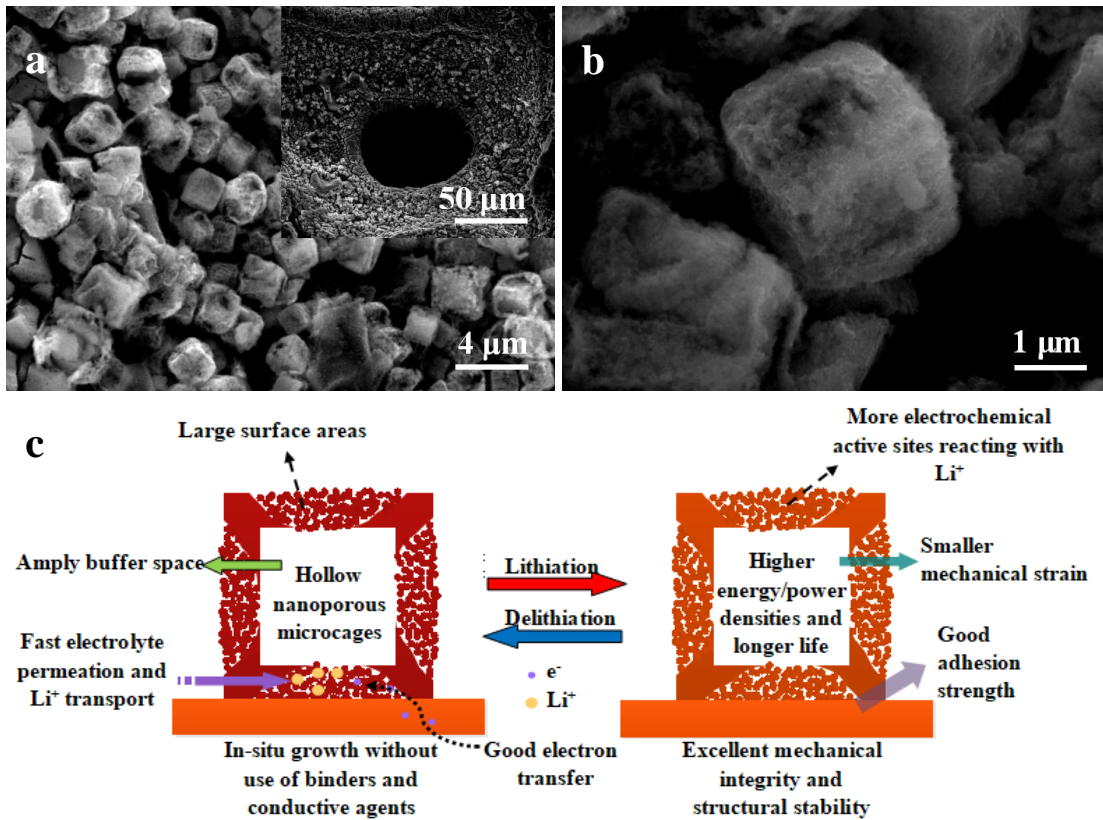
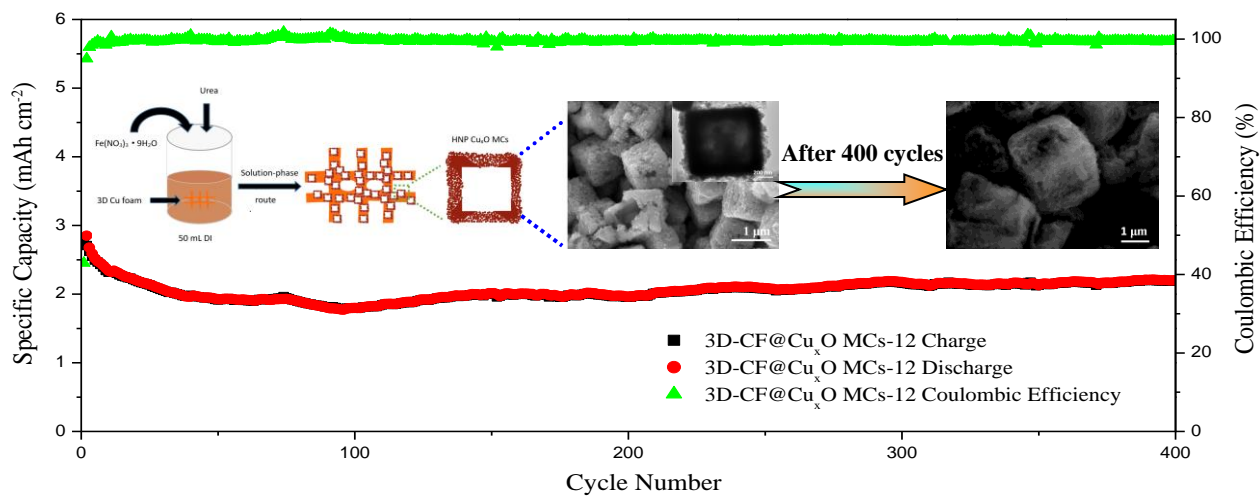


Fig. 4. Structure characterization after cycling and lithium storage mechanism of 3D-CF@Cu_xO MCs electrode. (a-b) SEM images of the 3D-CF@Cu_xO MCs-12 electrode after 400 charge-discharge cycles, in which the inset in part a is the corresponding low-magnification SEM image. (c) Schematic illustration for lithiation-delithiation reaction of the 3D-CF@Cu_xO MCs-12 electrode.

Table of Contents Image:



A facile one-step solution-phase route was developed to synthesize 3D-CF@Cu_xO MCs with superior Li storage properties towards renewable energy sources.